

DOI: 10.1002/cssc.201301123

Pt Nanocatalysts Supported on Reduced Graphene Oxide for Selective Conversion of Cellulose or Cellobiose to Sorbitol

Ding Wang,^[a, b] Wenqi Niu,^[b] Minghui Tan,^[b, c] Mingbo Wu,^{*[c]} Xuejun Zheng,^[a] Yanpeng Li,^[c] and Noritatsu Tsubaki^{*[b]}

Pt nanocatalysts loaded on reduced graphene oxide (Pt/RGO) were prepared by means of a convenient microwave-assisted reduction approach with ethylene glycol as reductant. The conversion of cellulose or cellobiose into sorbitol was used as an application reaction to investigate their catalytic performance. Various metal nanocatalysts loaded on RGO were compared and RGO-supported Pt exhibited the highest catalytic activity with 91.5% of sorbitol yield from cellobiose. The catalytic performances of Pt nanocatalysts supported on different carbon materials or on silica support were also compared. The results showed that RGO was the best catalyst support, and

the yield of sorbitol was as high as 91.5% from cellobiose and 58.9% from cellulose, respectively. The improvement of catalytic activity was attributed to the appropriate Pt particle size and hydrogen spillover effect of Pt/RGO catalyst. Interestingly, the size and dispersion of supported Pt particles could be easily regulated by convenient adjustment of the microwave heating temperature. The catalytic performance was found to initially increase and then decrease with increasing particle size. The optimum Pt particle size was 3.6 nm. These findings may offer useful guidelines for designing novel catalysts with beneficial catalytic performance for biomass conversion.

Introduction

Production of fuels or chemicals from renewable biomass resources instead of fossil resources has attracted great attention in recent years.^[1] Cellulose, a polysaccharide mainly composed of glucose via β -1-4 glycosidic linkage, exists widely in biomass resources.^[2] The conversion of cellulose into fuels or industrial chemicals can avoid potential conflicts with the food supply, a key issue in sustainable energy production.^[3] The utilization of cellulose is usually achieved through two steps: selective hydrolysis into glucose and further conversion into fuels and chemicals.^[4] Recently, the direct catalytic conversions of cellulose to sugar alcohol, ethylene glycol (EG), and gluconic acid have been reported.^[5–7] The sugar alcohols, especially sorbitol, are used not only as sweetener in diet foods, but also as an important basic chemical for the production of sustainable fuels and chemicals.^[8] Many catalysts, for example, Pt/ Al_2O_3 ,


Ru/carbon nanotubes, Ru/activated carbon, and Ni_xP , Pt/Na(H)-ZSM-5 have been used to convert cellulose or cellobiose into sorbitol directly.^[5,9–12] Nevertheless, few solid catalysts can obtain sorbitol with high yield when microcrystalline cellulose is used as feedstock except under harsh reaction conditions.^[9–11]

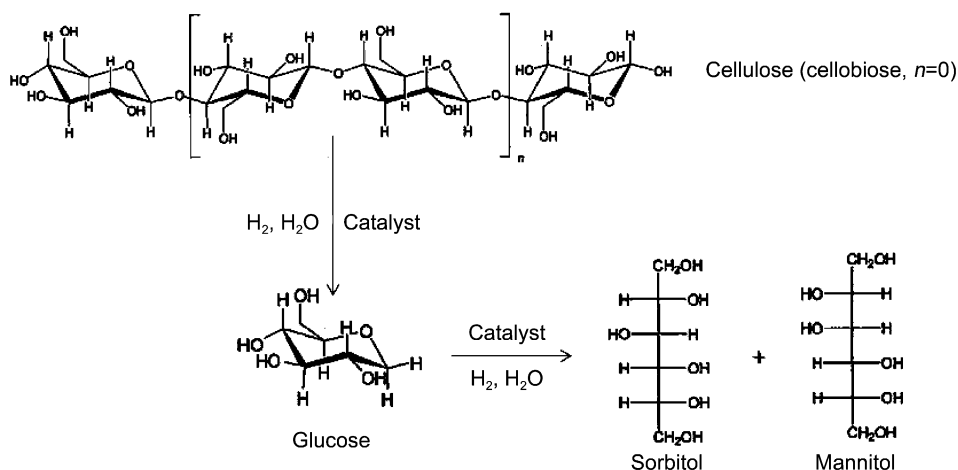
In the conversion of cellulose to sorbitol, the catalyst used can accelerate hydrolysis or/and hydrogenation reactions (Scheme 1). Carbon material is a good choice as the catalyst support due to its excellent stability under hydrothermal conditions and large surface area for dispersed active components.^[13] Carbon materials including activated carbon, mesoporous carbon and carbon nanotubes were reported as supports in the cellulose conversion reaction.^[5,10,13] However, to the best of our knowledge, graphene oxide, a novel carbon material, has not been reported as a catalyst or as support material in cellulose conversion. Compared with other carbon materials, graphene oxide, a one-atom thick planar sheet of hexagonally arrayed sp^2 carbon atoms, has attracted tremendous attention in recent years due to its relatively stable physical properties and its unique two-dimensional planar structure.^[14] In addition, graphene oxide is slightly acidic due to a large amount of surface functional groups.^[15,16] Carbon catalyst based on graphene oxide for facilitating oxidation and hydration reactions was reported.^[17] In addition, these abundant functional groups on the surfaces of graphene oxide can also be utilized as anchoring sites for loaded metal nanoparticles, which can increase the dispersion of the supported nanocatalysts and tune their catalytic performance. Furthermore, the graphene sheet has a spillover effect under reaction atmospheres (such as H_2 and

[a] Dr. D. Wang, Prof. X. Zheng
School of Materials Science and Engineering
University of Shanghai for Science and Technology
Shanghai 200093 (China)

[b] Dr. D. Wang, Dr. W. Niu, Dr. M. Tan, Prof. N. Tsubaki
Department of Applied Chemistry
Graduate School of Engineering, University of Toyama
Gofuku 3190, Toyama 930-8555 (Japan)
E-mail: tsubaki@eng.u-toyama.ac.jp

[c] Dr. M. Tan, Prof. M. Wu, Dr. Y. Li
State Key Laboratory of Heavy Oil Processing
China University of Petroleum
Shandong, Qingdao 266580 (PR China)
E-mail: wumb@upc.edu.cn

 Supporting Information for this article is available on the WWW under <http://dx.doi.org/10.1002/cssc.201301123>.



Scheme 1. Representation of the catalytic conversion of cellulose or cellobiose into sorbitol and mannitol.

O_2) especially when noble metal is the supported catalyst.^[17] These unique properties may be beneficial for the cellulose conversion if graphene oxide or its derivative is used as catalyst support.

The preparation method of catalysts directly influences their catalytic performance due to the intrinsic relationship between catalyst structure and reactivity. The nanoparticles loaded on graphene oxide have been reportedly prepared by physical methods such as electrostatic attraction, photoreduction, electrophoretic, or electrochemical deposition methods.^[18–20] These catalysts have also been prepared by chemical methods including hydrothermal/solvothermal method, ethylene glycol reduction, solid-state reaction method etc.^[21–23] Normally, these methods are complicated and time-consuming. A rapid and convenient method to prepare catalysts based on graphene-oxide-supported metal nanoparticles is needed.

In this present work, the catalyst prepared by a microwave-assisted reduction method was used in the conversion of cellulose or cellobiose. Cellobiose, a glucose dimer connected by a glycosidic bond, representing the simplest model molecule of cellulose,^[24] has been used in some experiments to investigate the catalytic performance or reaction mechanism of catalyst. Here, the catalytic performances of carbon materials [activated carbon (AC), graphene oxide (GO), reduced graphene oxide (RGO), carbon nanotubes (CNTs) and graphene (G)] were firstly studied. Then, various metal nanoparticles loaded on RGO were prepared and their catalytic performances were compared. Furthermore, the influence of supports on catalytic performance was researched. As the best catalyst, Pt/RGO catalyst was investigated in detail. Finally, the reaction mechanism was explored.

Results and Discussion

Catalytic performance of carbon materials

The carbon materials such as GO (preparation by modified Hummers method from expanded graphite),^[25] AC (after acid treatment), SiO_2 (ID-type gel supplied by Fuji Davison Chemical Ltd., specific surface area $270\text{ m}^2\text{ g}^{-1}$, pore volume $1.22\text{ cm}^3\text{ g}^{-1}$, average pore diameter 8.7 nm; after calcination at 773 K), G (prepared by thermal exfoliation of graphite oxide),^[26] and CNTs (after acid treatment)^[27] were

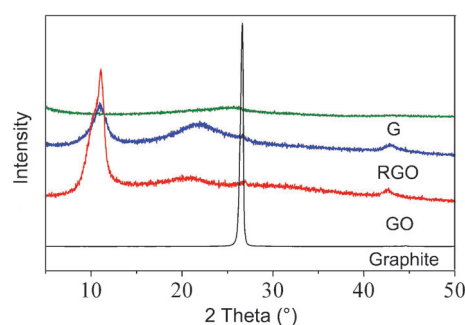


Figure 1. XRD patterns of graphite, graphene oxide (GO), reduced graphene oxide (RGO), and graphene (G).

chosen as catalysts to catalyze cellobiose to sugar alcohols. The XRD spectra in Figure 1 show the interlayer variations and the crystalline properties of graphite, GO, G, and RGO. Graphite shows a very sharp diffraction peak at $2\theta = 26.26^\circ$, corresponding to the interlayer spacing of 0.34 nm. The diffraction peak (2θ) around 11.6° belongs to the reflection of GO, and the interlayer spacing (0.80 nm) is much larger than that of pristine graphite owing to the introduction of oxygen-containing functional groups such as hydroxyl, epoxy, and carboxyl groups on the surface of graphite sheet.^[28] After reduction with the mixture of EG and water, the intensity of the typical diffraction peak (11.6°) of GO decreases and the position of the peak shifts to a higher angle, which is ascribed to the partial reduction of GO and the exfoliation of the layered GO nanosheets. The G prepared with thermal exfoliation of GO does not show any sharp peaks, demonstrating disorder and exfoliation. However, a broad and weak peak at 25.3° appears to show some amount of reclustered.^[29]

Figure 2 shows the reaction results of cellobiose conversion over various carbon materials. Without catalyst, cellobiose can be hydrolyzed with 89.2% of total conversion and 32.7% of glucose selectivity. The hydrolysis process in the conversion of

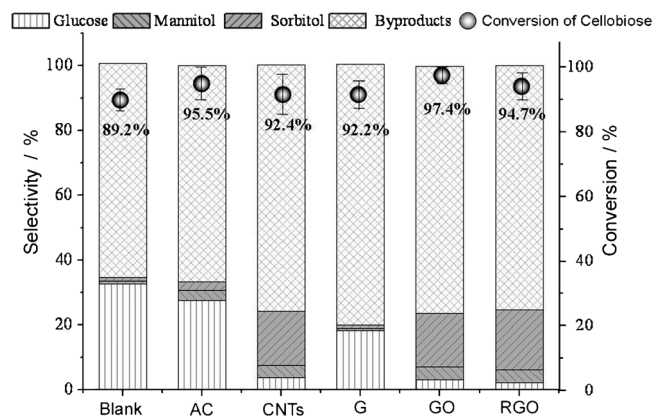


Figure 2. Catalytic conversions of cellobiose into sorbitol with carbon materials as catalyst. Reaction conditions: catalysts weight = 0.050 g; cellobiose weight = 0.171 g; reaction time = 3 h; temperature = 463 K; pressure = 5 MPa; H₂ as reaction gas.

cellobiose to glucose can be carried out even in the absence of catalyst, which may be due to H₃O⁺ formed by water autoprotolysis with the increase in temperature. These observations are in agreement with a recent investigation of cellulose hydrothermal degradation.^[30] The high conversion of cellobiose may be due to its simple molecular structure with a glucose dimer connected by a glycosidic bond. When carbon materials are employed as catalysts in the conversion of cellobiose, the conversion values are similar, but the product distribution is dependent on the type of carbon catalyst used. In Figure 2 and Table S1 in the Supporting Information, the byproducts include 5-HMF, low molecular polyols, and others. For AC and G catalysts, the primary by-product is 5-HMF, which is consistent with a previous study in which the chemistry for the decomposition pathways of cellulose and glucose in water indicates that glucose undergoes isomerization to form fructose, which can then undergo dehydration to form HMF.^[31] For CNTs, GO, and RGO catalysts, the yield of HMF is decreased whereas the yields of hexitol and low molecular polyols including xylitol, erythritol, glycerol, and ethylene glycol are increased. For GO or RGO catalysts, the increased sorbitol yield may be due to the oxygen-containing functionalities (alcohols, epoxides, and carboxylates), their unique structure, and defects in the graphene sheets.^[32] The GO and RGO catalysts for acid catalysis or hydrogenation were also reported to be active for epoxides ring opening in the case of GO and nitrobenzene hydrogenation in the case of RGO.^[33,34] As seen in Figure 2, the catalytic performance of RGO is similar to that of GO, which indicates that the catalytic activity is not influenced by the GO reduction process. However, the yield of sorbitol on GO or RGO is also low. Therefore, it is necessary to load hydrogenation catalysts onto these carbon materials to improve their catalytic performance.

Catalytic performance of different metal nanocatalysts supported on RGO

The typical hydrogenation catalysts such as Ni, Cu, Pd, Rh, Ru, and Pt were loaded on RGO to improve the cellobiose conver-

sion and the yield of sorbitol. All the catalysts were prepared by the same EG reduction method with the assistance of microwave heating (Scheme S1). The advantage of microwave heating over other conventional heating methods is that heating is uniform and rapid, which dramatically reduces processing time, increases product yield, and enhances product purity and properties.^[35] Furthermore, the employment of microwave radiation as a heat source has been demonstrated to provide unique effects such as “superheating” of solvents above their boiling point and the selective heating of strongly microwave-absorbing materials, which can increase the metal loading effi-

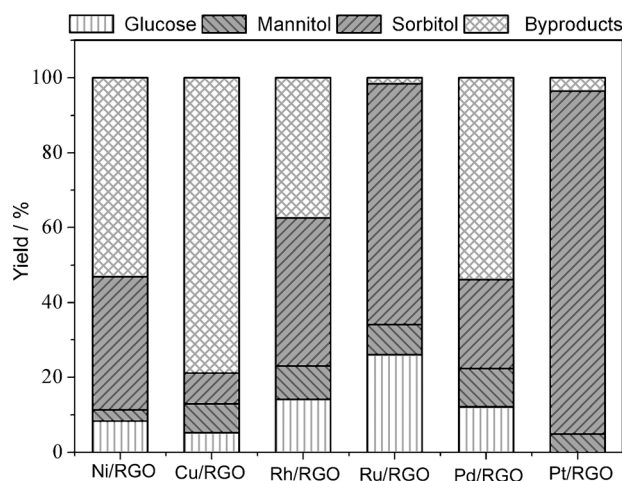


Figure 3. Catalytic performance of different metal catalyst (10 wt% Ni, 10 wt% Cu, 5 wt% Rh, 5 wt% Ru, 5 wt% Pd, 5 wt% Pt) supported on RGO catalyst for cellobiose conversion to sorbitol. Reaction conditions: catalyst weight = 0.050 g; cellobiose weight = 0.171 g; reaction time = 3 h; temperature = 463 K; pressure = 5 MPa; H₂ as reaction gas.

ciency.^[36] As shown in Figure 3, all the catalysts demonstrate almost 100% conversion of cellobiose. The different product distributions are influenced by the synergistic effect between the loaded metal and RGO. The order of sorbitol yield is as follows: Pt/RGO > Ru/RGO > Rh/RGO > Ni/RGO > Pd/RGO > Cu/RGO. The highest sorbitol yield together with no production of glucose is obtained for Pt/RGO, which indicates that Pt is the most suitable catalyst with the highest sorbitol yield of approximately 91.5%.

Catalytic performance of Pt nanocatalysts on different supports

In order to clarify the effect of different supports on the conversion of cellobiose to sorbitol, Pt, the best active metal as above-mentioned, was also loaded on other supports. We used TGA to determine the Pt loading amounts on various carbon catalysts but there was no significant change, which means that the catalytic activity of Pt loaded on different carbon supports is comparable. As shown in Figure 4, the cellobiose conversion is as high as 100%. The yield to sorbitol is only 41.9% when Pt nanoparticles are used as catalyst. Compared with Pt nanoparticles prepared by the same

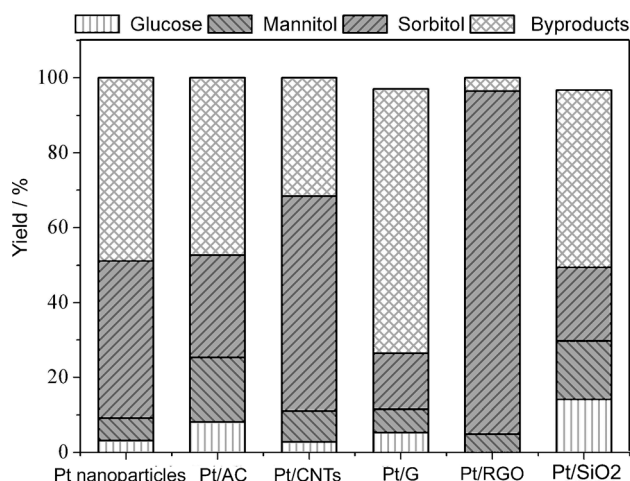


Figure 4. Catalytic performance of Pt loaded on different supports for cellobiose conversion to sorbitol. Reaction conditions: catalyst weight = 0.050 g (Pt nanoparticles, 0.0025 g); cellobiose weight = 0.171 g; reaction time = 3 h; temperature = 463 K; pressure = 5 MPa; H₂ as reaction gas.

method, the yield of sorbitol is improved from 41.9% to 91.5% when RGO is used as the Pt support. Note that not all support materials could improve the catalytic performance. From Figure 4, it is clear that equal amounts of Pt loaded, the levels of catalytic activity have the following order: Pt/RGO > Pt/CNT > Pt nanoparticles > Pt/AC > Pt/SiO₂ > Pt/G.

The XRD patterns of Pt nanoparticles loaded on different supports are displayed in Figure S1. The strong diffraction peaks at $2\theta = 39.6^\circ$, 46.2° , and 67.5° can be assigned to the characteristic (111), (200), and (220) crystalline planes of Pt. The average crystallite sizes were calculated by the Scherrer equation at 39.6° , which is shown in Table 1. Moreover, the morphology of Pt nanoparticles and Pt nanoparticles loaded on different supports was investigated by TEM. As in Figure S2, the dispersion and particle sizes of Pt are dependent on support type. The particle size distribution in Figure S2 and Table 1 shows that the average size of Pt nanoparticles is about 3.5 nm for Pt nanoparticles, 3.6 nm for Pt/AC, 3.1 nm for Pt/CNTs, 1.2 nm for Pt/G, 3.6 nm for Pt/RGO, and 3.1 nm for Pt/SiO₂. The dispersion and exposed surface area of the Pt nanoparticles were determined by chemisorption of CO. As shown

Catalyst	Exposed Pt surface area ^[a] [m ² g ⁻¹]	Pt dispersion ^[a] [%]	Particle size ^[b] [nm]	Crystallite sizes ^[c] [nm]
Pt/SiO ₂	65.2	26.4	3.1	2.9
Pt/AC	33.9	13.7	3.6	7.7
Pt/CNTs	31.6	12.8	3.1	4.0
Pt/G	8.7	3.5	1.2	— ^[d]
Pt/RGO	79.2	32.3	3.6	3.6

[a] The surface area was determined by CO chemisorption. [b] The average size of nanoparticles was evaluated from counting and averaging TEM images. [c] The average crystallite sizes were calculated from XRD pattern by using the Scherrer equation at 39.6° . [d] The diffraction peak was too low to estimate.

in Table 1, the Pt exposed surface area and dispersion of catalyst also depend on the type of support. The Pt amounts of exposed surface area and dispersion have the following order: Pt/RGO > Pt/SiO₂ > Pt/AC > Pt/CNTs > Pt/G. The catalyst with greater exposed surface area and dispersion of Pt usually shows higher conversion in hydrogenation reaction.^[31,37] Normally, the metallic catalyst with small metal particle size possesses high dispersion and high catalytic activity. Why are the Pt dispersion and the catalytic activity for Pt/G are so low? The low catalytic activity of Pt/G catalyst may be due to the high oxidation states of the metal catalyst on G support. As shown in Figure S3, Pt 4f spectra of Pt/G show that the main valences of Pt are Pt²⁺ and Pt⁴⁺. However, the Pt⁰ is the active site in the cellobiose conversion reaction (Scheme 1). The oxidation state of Pt can be attributed to the reoxidation of oxygen in air. The high oxidation state may be also the reason that the Pt dispersion on Pt/G catalyst is so low. Compared with Pt/AC, the Pt/CNTs catalyst with similar Pt dispersion has better catalytic performance, which may be due to the following reasons: Firstly, most pores in AC are micropores, and are too small for cellobiose to enter.^[32,38] Secondly, as in Figure 2, CNTs with lots of surface functional groups formed by acid pretreatment have high sorbitol yield and low glucose yield, indicating that the CNTs have higher catalytic activity than AC in this reaction. With high Pt dispersion, Pt/SiO₂ has the lowest catalytic performance and this may be due to the same reason as for Pt/AC. Therefore, the high catalytic activity is attributed to the synergistic effects of supports and the supported Pt nanoparticles. As in Figure 4, Pt loaded on RGO shows the highest catalytic performance, which indicates that RGO is the best support for the conversion of cellobiose to sorbitol.

The effect of Pt particle size on the catalytic performance

To disclose the effect of Pt particle size on the catalytic activity, Pt/RGO catalysts with different Pt particle sizes were prepared through the same reduction method. In this microwave-assisted method, Pt particle size can be controlled with different temperature treatments. The XRD patterns of GO and Pt/RGO after different heat treatments are shown in Figure 5. It can be seen that the typical diffraction peak (002) of GO at 11.6° shifts to higher angle after the loading of Pt nanoparticles on RGO with a treatment temperature above 403 K; this indicates that the GO is converted to RGO. The strong diffraction peaks at $2\theta = 39.6^\circ$, 46.2° , and 67.5° can be assigned to the characteristic (111), (200), and (220) crystalline planes of Pt, respectively. Pt possesses face-centered-cubic (fcc) structure. The diffraction peak of Pt (111) is used to estimate the Pt particle size by the Scherrer equation. The calculated average particle sizes of Pt on GO sheets are 2.0 nm for Pt/RGO-403 K, 2.7 nm for Pt/RGO-413 K, 3.6 nm for Pt/RGO-433 K, and 4.3 nm for Pt/RGO-453 K.

Figure 6 shows the TEM images and Pt particle size distributions of Pt/RGO-T. All TEM images demonstrate that graphene nanosheets are uniformly decorated by distributed Pt nanoparticles with few aggregations, indicating a strong interaction between the graphene support and Pt particles. The mean size of

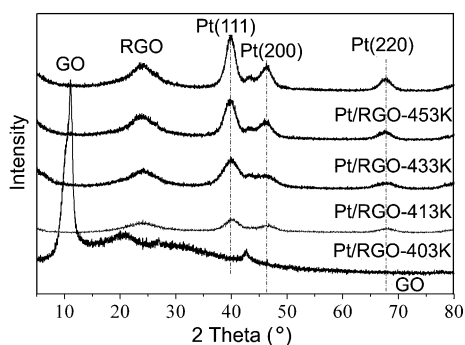


Figure 5. XRD patterns of GO and Pt/RGO-T ($T = 403, 413, 433, 453$ K).

Pt nanoparticles is very consistent with the value estimated by the Scherrer equation from Figure 5.

As shown in Figure 7, the yield of sorbitol increases with the mean size of Pt up to 3.6 nm and then decreases on further increase in Pt particle size. The highest catalytic performance is obtained by the Pt/RGO-433 catalyst with 91.5% sorbitol yield. A similar trend is also observed when the cellobiose is replaced by cellulose (see Scheme 1). The highest yield of hexitol is 69% (58.9% of sorbitol and 10.1% of mannitol). The results show

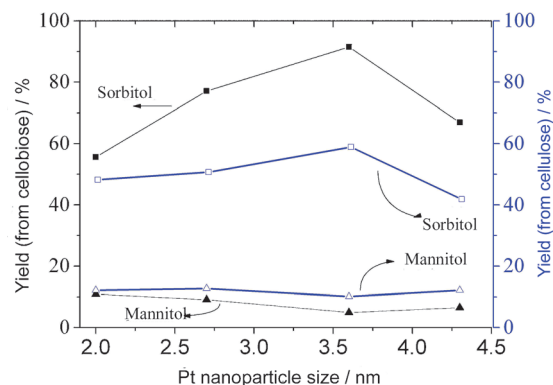


Figure 7. Conversions of cellobiose and cellulose into sorbitol and mannitol by Pt/RGO-T catalysts with different particle size ($T = 403, 413, 433, 453$ K). Reaction conditions: catalyst weight = 0.050 g; cellulose or cellobiose weight = 0.171 g; reaction time = 24 h for cellulose and 3 h for cellobiose; temperature = 463 K; pressure = 5 MPa; H_2 as reaction gas.

that the Pt particle size is one of the critical factors affecting the cellulose conversion. In addition, the catalytic activity may also be affected by the different microwave temperatures at which the RGO supports are processed.

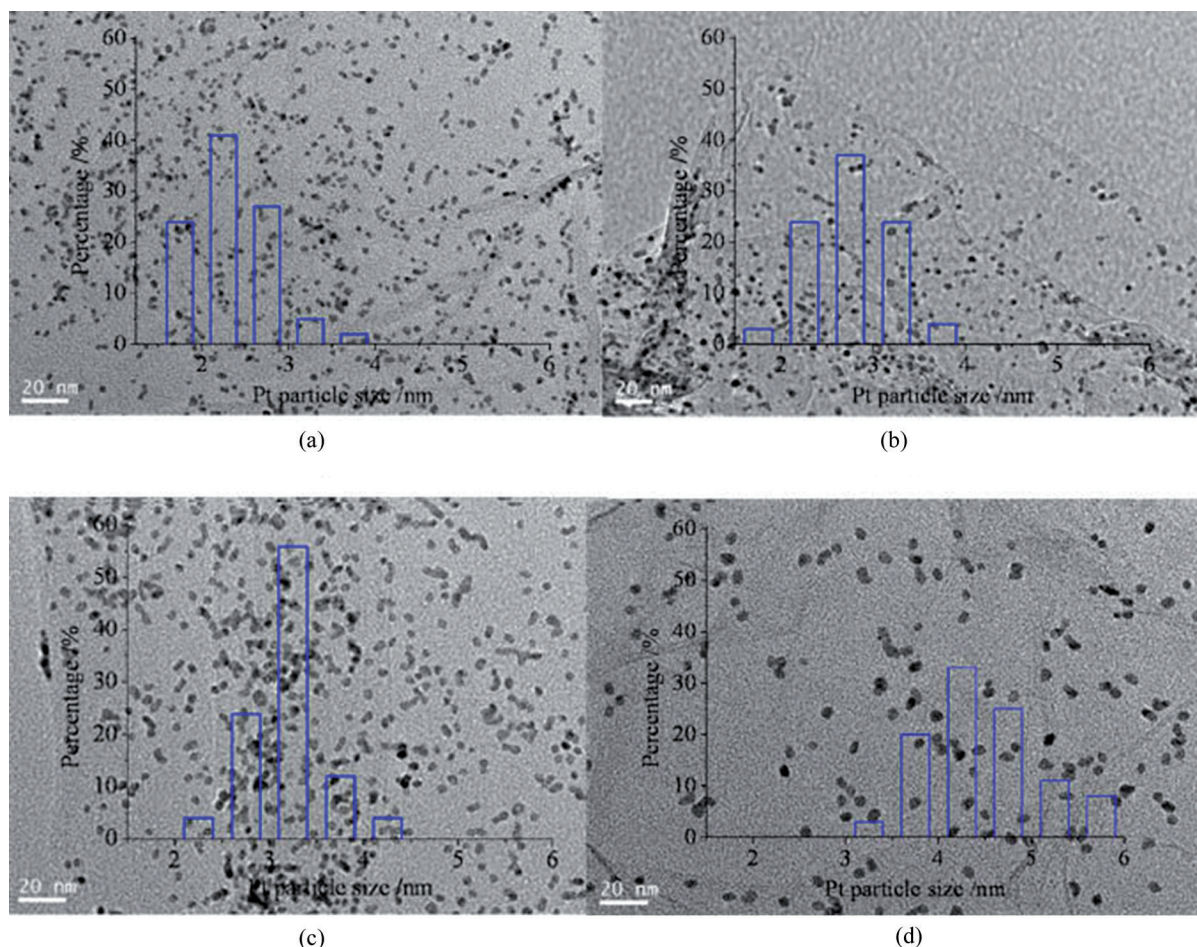


Figure 6. TEM images and particle size distribution of Pt/RGO-T, at temperatures of (a) 403, (b) 413, (c) 433, and (d) 453 K.

Characterization of Pt/RGO catalyst

The preparation, physicochemical properties, and the catalytic performances of Pt/RGO catalyst with the highest catalytic activity were systematically investigated. The morphology of RGO and as-prepared Pt/RGO were characterized by means of TEM. As shown in Figure 8a, the surface of RGO is smooth and free from any contaminating particulate, which indicates that few layered graphene oxides are formed, although the TEM image cannot estimate the layer numbers of the graphene oxide nanosheets exactly. As in Figure 8b, highly monodispersed Pt nanoparticles with a uniform size of 3.6 nm decorated on RGO surface are obtained by simple and rapid microwave heating of H_2PtCl_6 and GO in the mixture of EG and water. The most significant feature here is that the Pt nanoparticles with a uniform size (3.6 nm) are monodispersed on the surface of graphene oxide (as shown in Figure 8b and c). Figure 8d shows a high-resolution TEM image of Pt/RGO. The measured interplanar spacing of the particle lattice is 0.23 nm, which corresponds to the (111) crystal plane of Pt nanoparticles shown in X-ray diffraction (XRD) data (Figure 5). These TEM images confirm that the highly monodispersed Pt nanoparticles with uniform size can be successfully synthesized and well dispersed on RGO sheets by the microwave-assisted reduction method. Compared with previous researches,^[18–20] Pt nanoparticles on graphene oxide sheets seem to be highly monodispersed with smaller uniform size. Furthermore, the Pt/RGO catalyst prepared by the microwave-assisted reduction method is shown to possess a “fluffy” morphology and its surface area is $180.2 \text{ m}^2\text{g}^{-1}$. The surface area is relatively low compared to the surface area of the single graphene sheet,^[20] indicating a certain degree of restacking of the graphene sheets.

X-ray photoelectron spectra (XPS) was used to investigate the surface composition of RGO and Pt/RGO catalysts. As shown in Figure 9, the C1s core level for RGO still shows a high degree of oxidation, which consists of three main components assigned to the C–C (sp^3 carbon, 285.8 eV), C–C (sp^2 carbon, 284.5 eV), C–O (hydroxyl, 286.6 eV), and C=O (carbonyl, 288.4 eV) groups.^[39] The large amount of residual functional groups including C–O in RGO indicate that GO was only partly reduced by EG solution. After the introduction of H_2PtCl_6 , it is clearly shown that the peak associated with C–C bond (284.5 eV) becomes predominant while the additional peak of C–O (286.6 eV) decreases tremendously, suggesting most oxygen-containing functional groups

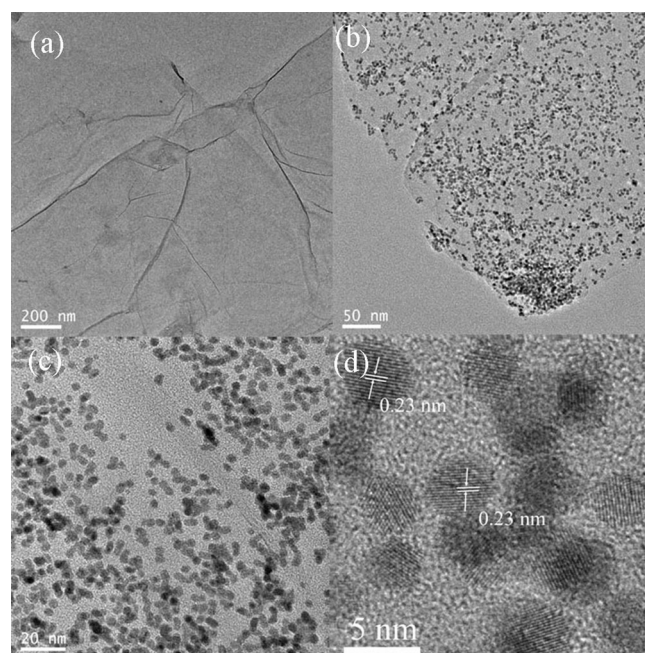


Figure 8. TEM images of (a) RGO, (b, c) Pt/RGO, and (d) high-resolution transmission electron microscopy (HR-TEM) image of Pt/RGO.

have been removed. These findings indicate that the addition of H_2PtCl_6 plays an important role in the formation of RGO. Figure 9c shows the O1s XPS spectra of RGO and Pt/RGO nanocomposites. The decrease of oxygen-containing functional groups can also be seen from the decreasing peaks of C–O and C=O. Pt4f spectra of Pt/RGO show the expected doublets for $\text{Pt}4f_{7/2}$ and $\text{Pt}4f_{5/2}$, with Pt^0 , Pt^{2+} , and Pt^{4+} oxidation states

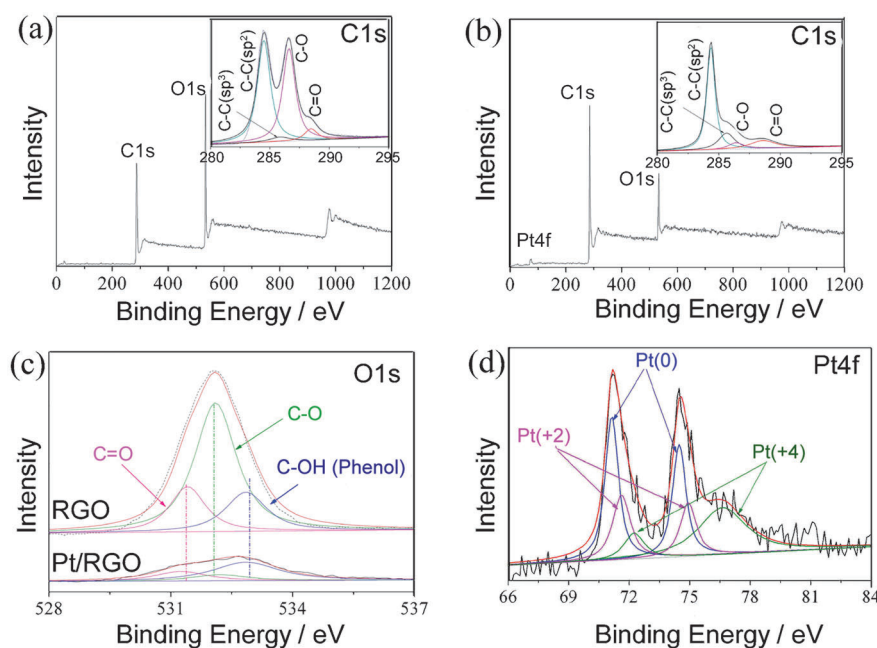


Figure 9. Typical XPS spectra of RGO and Pt/RGO: (a) survey spectra and C1s of RGO, (b) survey spectra and C1s of Pt/RGO, (c) O1s region XPS spectra, and (d) Pt4f region XPS spectra.

(Figure 9d). It is interesting to note that a significant percentage of Pt remains in its native state (Pt^0) in Pt/RGO. In addition, two different types of Pt (Pt^{2+} and Pt^{4+}) can be assigned, which suggests that oxygen linkages exist between the Pt nanoparticles and the RGO surface, and between the Pt nanoparticles and the oxide layers formed on the Pt surface. The small Pt nanoparticles are formed by the anchorage of Pt ions on the graphene oxide surface and by their subsequent reduction to fine particles without obvious agglomeration.

Catalytic performances of Pt/RGO catalyst

The effect of the reaction temperature on the catalytic performance of Pt/RGO catalyst is given in Figure 10. It can be seen that the conversion of cellobiose increases from 75.2% to 100% on increasing the temperature from 423 K to 463 K. The sorbitol yield increases simultaneously and reaches a maximum at 463 K, then decreases on further increasing the temperature to 483 K. It is thought that a high temperature causes cellobiose to be partially carbonized and that the produced sorbitol can be converted further to other undesirable byproducts. Consequently, the optimum reaction temperature is 463 K.

Using the milled cellulose as the raw material, the experimental conditions such as the reaction temperature, the reaction pressure, the reaction time, and the Pt concentration were investigated. As shown in Figure 11a, the yield of sorbitol is very low at 423 K. Compared with Figure 10, the low temperature might be not helpful to the hydrolysis of cellulose. The yield of sorbitol and the conversion of cellulose increase with increasing temperature. However, the sorbitol yield is relatively low when the reaction temperature is 483 K, which might be due to the partial decomposition or dehydration of products and the generation of some byproducts, such as low-molecular-weight polyols, sorbitan, isosorbide, CO, and CH_4 . The influence of reaction pressure is shown in Figure 11b, from which it can be seen that the conversion of cellulose increases with increasing pressure. Furthermore, the pressure also influences the yield of sorbitol. Higher pressure results in an increase in sorbitol yield. The reaction time is also found to be important in this reaction, as shown in Figure 11c. The conversion of cellulose (36.3%) and sorbitol yield are very low with a reaction time of 1 h. However, the conversion of cellobiose is as high as 100% when the reaction time is 3 h (Figure 10). The cello-

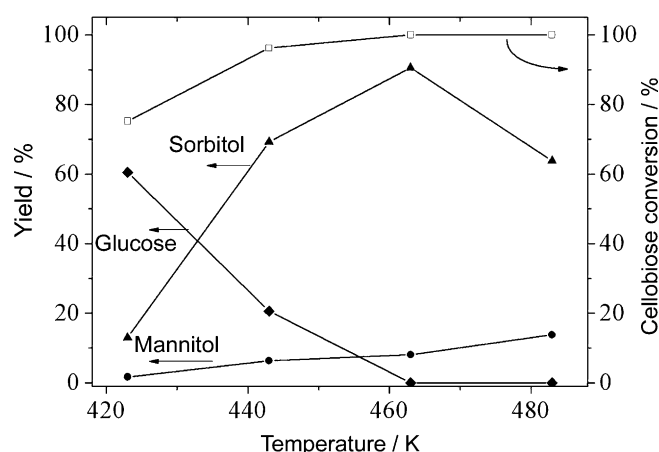


Figure 10. Influence of the reaction temperature on the conversion of cellobiose to sorbitol. Reaction conditions: catalyst weight = 0.050 g; cellobiose weight = 0.171 g; reaction time = 3 h; temperature = 423–483 K; pressure = 5 MPa; H_2 as reaction gas.

biose can be easily hydrolyzed compared with cellulose, indicating that the hydrolysis of cellulose is the rate determining step. The effect of level of Pt loading in the Pt/RGO catalyst is also studied. The yield of sorbitol can be increased from 24.9% to 58.9% on increasing Pt loading from 1 wt% to 5 wt%.

In order to study the stability of the Pt/RGO catalyst, the catalyst was characterized with TEM after a 24 h reaction. As shown in Figure S4, the average size of Pt nanoparticles on the

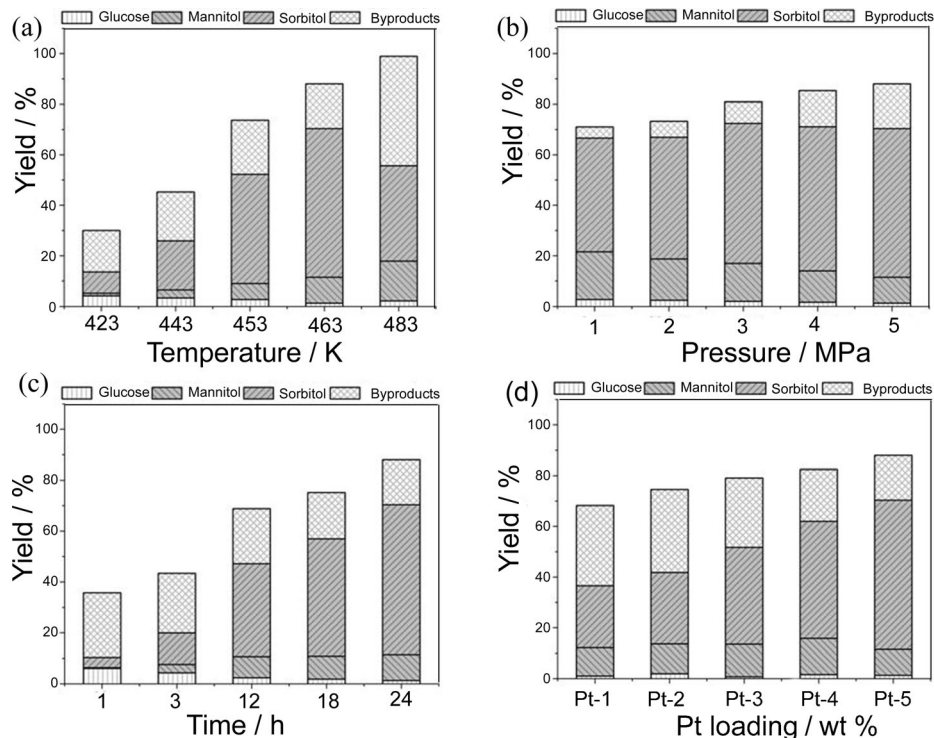


Figure 11. Influences of (a) reaction temperature, (b) reaction pressure, (c) reaction time, and (d) Pt loading amount on the conversion of cellulose to sorbitol. Reaction conditions: catalyst weight = 0.050 g; cellulose weight = 0.171 g; H_2 as reaction gas; temperature = 463 K (in (a) 423–483 K); pressure = 3 MPa (in (b) 1–5 MPa); reaction time = 24 h (in (c) 1–24 h); Pt loading amount = 5% (in (d) 1–5%).

used Pt/RGO catalyst is similar to that on the fresh one. Particle aggregation is not observed in the TEM image, suggesting that the catalyst is very stable and can be reused. As shown in Figure 12, the reusability is also indicated by the similar sorbitol selectivity achieved on using the used Pt/RGO as catalyst and fresh cellulose as reactant. The slight decrease of cellulose conversion after several runs might be due to the loss of catalysts during the transfer process.

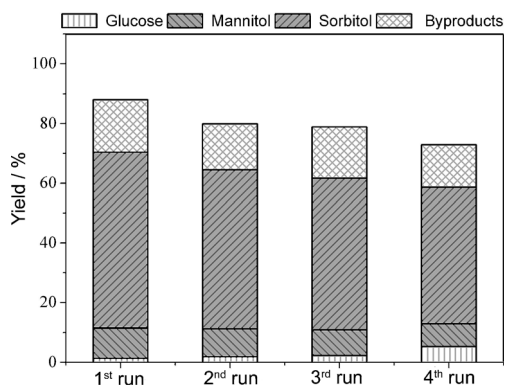


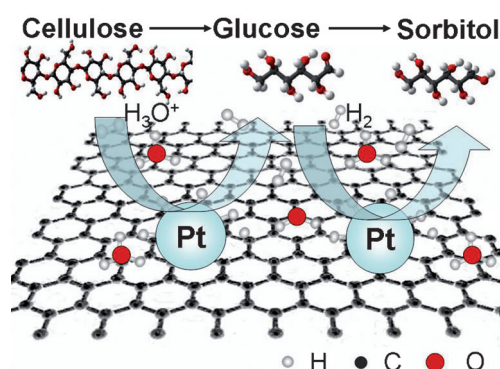
Figure 12. Reuse experiments of Pt/RGO catalyst for cellulose conversion. Reaction conditions: catalysts weight = 0.050 g; cellulose weight = 0.171 g, reaction time = 24 h; temperature = 463 K; pressure = 5 MPa; H₂ as reaction gas.

Reaction mechanism of cellulose conversion

The enhanced catalytic performance of the Pt/RGO catalyst for the conversion of cellulose to sorbitol may be due to the following reasons: The increase in utilization efficiencies of platinum nanocatalysts on RGO supports can be attributed to the enlarged surface area and the well-dispersion of the RGO supports and catalyst. The optimum size of Pt particles and the exposed crystal plane are beneficial for the hydrogenation of reactants. Pt on RGO promotes the protonations of water, which is due to the hydrogen molecules spilt over to create in situ acid sites and to catalyze hydrolysis of cellulose or cellobiose (Scheme 2). The intermediate glucose or other oligosaccharides can be selectively hydrogenated to sorbitol on the highly active Pt nanoparticles. Therefore, in the conversion of sugars to sorbitol, the RGO supports highly dispersed Pt nanoparticles by means of an anchoring effect, maintains surface acidity through H₂ spillover from Pt, catalyzes hydration reaction through its acidic sites, and suppresses the formation of by-products.

Conclusions

Pt/RGO catalyst is prepared by microwave-assisted EG reduction method, which presents high activity and selectivity for the conversion of cellobiose or cellulose to sorbitol. The structure and the catalytic performance of Pt/RGO catalyst are systematically investigated. The high catalytic activity is attributed to the synergistic effects of supports and the supported Pt nanoparticles. The results show that the graphene oxide



Scheme 2. Conversion mechanism of cellulose to sorbitol catalyzed by Pt/RGO.

sheets act as an excellent support and stabilizer for the very finely dispersed Pt nanoparticles, preventing nanoparticle aggregation. The sorbitol yield is as high as 91.5% or 58.9% when cellobiose or cellulose are employed as the reactant, respectively. The optimum particle size of Pt is 3.6 nm and the optimum reaction temperature is 463 K. The improvement of catalytic activity is attributed to the hydrogen spillover effects of the Pt/RGO catalyst.

Experimental Section

Catalyst preparation

The support materials included GO,^[25] AC (after acid treatment), SiO₂ (ID, after calcination at 773 K), G (prepared by thermal exfoliation of graphite oxide.^[26]), CNTs (after acid treatment).^[27] For further details, please see the Supporting Information.

EG reduction with the assistance of microwave radiation was applied to load metallic nanoparticles on RGO or on other support materials. Metal salt solution, such as H₂PtCl₆, RuCl₃, H₂PdCl₆, Ni(NO₃)₂, or Cu(NO₃)₂ solution, was chosen as metal source to prepare the metallic nanoparticles. For example, in a typical synthesis of Pt/RGO catalyst, the GO and H₂PtCl₆ were dispersed in EG solution with the assistance of ultrasonic treatment. After being ultrasonically treated for 30 min, the mixture was then put into an automated focused microwave system and treated at 393–453 K for 30 min. The catalysts were obtained through a redox reaction heated by microwave. The reduction reaction could be observed by a color change from yellow GO in the mixture of EG and aqueous solution, to dark black after 30 min of microwave heating. The solid products were then collected by filtration and washed with deionized water as well as ethanol and were then dried. The metal loading in all catalysts was 5 wt%. The obtained catalyst was defined as M/RGO. RGO was prepared by the same method as above, but without the addition of metal salt. Pure Pt nanoparticles were prepared from the same EG reduction method without the existence of supports.

Characterization of catalysts

The morphologies of the samples were characterized with a high resolution TEM (JEOL JEM-2100 UHR) operated at 200 kV. The crystal structure of the materials was confirmed by means of XRD using a Rigaku D/max-2550 V diffractometer employing CuK_α radi-

tion ($\lambda = 1.54 \text{ \AA}$; scanning rate: $0.02^\circ/\text{s}$). XPS was conducted using an ESCALAB 250Xi spectrometer equipped with a pre-reduction chamber. The position of the C1s peak (284.5 eV) was used to correct the XPS binding energies for all catalysts for possible charging effects. Thermal analysis was carried out on a DTG-60 (Shimadzu) in air flow. The loading amount of Pt was analyzed by means of an inductive coupled plasma emission spectrometer (Shimadzu ICPE-9000). The metal dispersion and metal surface area was determined by CO chemisorption using a pulse chemisorption mode (BELCAT, BEL Japan, Inc.). Samples were treated in He flow by increasing the temperature to 423 K at 5 K min^{-1} and holding at 423 K for 1 h. Samples were then heated to 673 K at 10 K min^{-1} and reduced in 10% H_2/Ar at 673 K for 1 h. Chemisorbed hydrogen was removed by treatment in He flow at 493 K for 1 h. Samples were then exposed to pulses of 5% CO/He . CO concentration was measured using a thermal conductivity detector. Dispersions, defined as the fraction of Pt atoms exposed at surfaces, were determined by assuming a 1:1 ratio of CO molecules to surface Pt atoms.

Catalytic reaction

The conversion of cellobiose or cellulose was performed with a batch-type high-pressure autoclave reactor. Typically, 0.050 g catalyst and 0.171 g cellulose (after ball milling for 4 days) or cellobiose were loaded into the reactor precharged with 20 mL H_2O . The reactor H_2 pressure was maintained at 5 MPa at room temperature, and then the reaction was conducted at 463 K for 3 h. After reaction, the solid phase was separated by centrifugation, and the liquid products were analyzed with HPLC (Waters Assoc, USA). Cellulose conversion was determined as reported by the weight difference of dried cellulose before and after the reaction.^[5] The cellobiose conversion was calculated by means of the HPLC results before and after the reaction. The product selectivity was calculated based on the carbon basis (calculated by dividing the amount of carbon found in a particular product by the amount of carbon found in the products). The product yield was calculated as follows: $\text{yield}(\%) = (\text{weight of product})/(\text{weight of cellulose or cellobiose charged in reactor})$.

Acknowledgements

M.T. thanks the China Scholarship Council (CSC) for financial support.

Keywords: biomass · graphene oxide · hydrogen spillover effect · hydrogenation · sorbitol

- [1] A. M. Ruppert, K. Weinberg, R. Palkovits, *Angew. Chem. Int. Ed.* **2012**, *51*, 2564–2601; *Angew. Chem.* **2012**, *124*, 2614–2654.
- [2] M. S. Mettler, S. H. Mushrif, A. D. Paulsen, A. D. Javadekar, D. G. Vlachos, P. J. Dauenhauer, *Energy Environ. Sci.* **2012**, *5*, 5414–5424.
- [3] K. Kohse-Höinghaus, P. Oßwald, T. A. Cool, T. Kasper, N. Hansen, F. Qi, C. K. Westbrook, P. R. Westmoreland, *Angew. Chem. Int. Ed.* **2010**, *49*, 3545–3545; *Angew. Chem.* **2010**, *122*, 3625–3625.
- [4] H. Kobayashi, H. Ohta, A. Fukuoka, *Catal. Sci. Technol.* **2012**, *2*, 869–883.
- [5] C. Luo, S. Wang, H. Liu, *Angew. Chem. Int. Ed.* **2007**, *46*, 7636–7639; *Angew. Chem.* **2007**, *119*, 7780–7783.

- [6] D. An, A. Ye, W. Deng, Q. Zhang, Y. Wang, *Chem. Eur. J.* **2012**, *18*, 2938–2947.
- [7] N. Ji, T. Zhang, M. Zheng, A. Wang, H. Wang, X. Wang, J. G. Chen, *Angew. Chem. Int. Ed.* **2008**, *47*, 8510–8513; *Angew. Chem.* **2008**, *120*, 8638–8641.
- [8] L. N. Ding, A. Q. Wang, M. Y. Zheng, T. Zhang, *ChemSusChem* **2010**, *3*, 818–821.
- [9] A. Fukuoka, P. L. Dhepe, *Angew. Chem. Int. Ed.* **2006**, *45*, 5161–5163; *Angew. Chem.* **2006**, *118*, 5285–5287.
- [10] H. Wang, L. Zhu, S. Peng, F. Peng, H. Yu, J. Yang, *Renewable Energy* **2012**, *37*, 192–196.
- [11] P. Yang, H. Kobayashi, K. Hara, A. Fukuoka, *ChemSusChem* **2012**, *5*, 920–926.
- [12] S. You, I. Baek, Y. Kim, K.-E. Jeong, H.-J. Chae, T.-W. Kim, C.-U. Kim, S.-Y. Jeong, T. Kim, Y.-M. Chung, S.-H. Oh, E. Park, *Korean J. Chem. Eng.* **2011**, *28*, 744–750.
- [13] J. Pang, A. Wang, M. Zheng, Y. Zhang, Y. Huang, X. Chen, T. Zhang, *Green Chem.* **2012**, *14*, 614–617.
- [14] C. Huang, C. Li, G. Shi, *Energy Environ. Sci.* **2012**, *5*, 8848–8868.
- [15] X. Chu, Q. Zhu, W.-L. Dai, K. Fan, *RSC Adv.* **2012**, *2*, 7135–7139.
- [16] A. Dhakshinamoorthy, M. Alvaro, P. Concepcion, V. Fornes, H. Garcia, *Chem. Commun.* **2012**, *48*, 5443–5445.
- [17] D. R. Dreyer, H.-P. Jia, C. W. Bielawski, *Angew. Chem. Int. Ed.* **2010**, *49*, 6813–6816; *Angew. Chem.* **2010**, *122*, 6965–6968.
- [18] J. Zhu, Y. K. Sharma, Z. Zeng, X. Zhang, M. Srinivasan, S. Mhaisalkar, H. Zhang, H. H. Hng, Q. Yan, *J. Phys. Chem. C* **2011**, *115*, 8400–8406.
- [19] Z. Sun, X. Lu, *Ind. Eng. Chem. Res.* **2012**, *51*, 9973–9979.
- [20] J. Wang, T. Tsuzuki, B. Tang, X. Hou, L. Sun, X. Wang, *ACS Appl. Mater. Interfaces* **2012**, *4*, 3084–3090.
- [21] M.-S. Wu, Y.-P. Lin, C.-H. Lin, J.-T. Lee, *J. Mater. Chem.* **2012**, *22*, 2442–2448.
- [22] S. Wu, Q. He, C. Zhou, X. Qi, X. Huang, Z. Yin, Y. Yang, H. Zhang, *Nano-scale* **2012**, *4*, 2478–2483.
- [23] Y. Li, W. Gao, L. Ci, C. Wang, P. M. Ajayan, *Carbon* **2010**, *48*, 1124–1130.
- [24] N. Yan, C. Zhao, C. Luo, P. J. Dyson, H. Liu, Y. Kou, *J. Am. Chem. Soc.* **2006**, *128*, 8714–8715.
- [25] W. S. Hummers, R. E. Offeman, *J. Am. Chem. Soc.* **1958**, *80*, 1339–1339.
- [26] A. Kaniyoor, T. T. Baby, S. Ramaprabhu, *J. Mater. Chem.* **2010**, *20*, 8467–8469.
- [27] D. Wang, G. Yang, Q. Ma, M. Wu, Y. Tan, Y. Yoneyama, N. Tsubaki, *ACS Catal.* **2012**, *2*, 1958–1966.
- [28] J. Li, H. Lin, Z. Yang, J. Li, *Carbon* **2011**, *49*, 3024–3030.
- [29] Y. Guo, C. Bao, L. Song, B. Yuan, Y. Hu, *Ind. Eng. Chem. Res.* **2011**, *50*, 7772–7783.
- [30] V. Jollet, F. Chambon, F. Rataboul, A. Cabioc, C. Pinel, E. Guillon, N. Es-sayem, *Green Chem.* **2009**, *11*, 2052–2060.
- [31] W. Deng, R. Lobo, W. Setthapun, S. T. Christensen, J. W. Elam, C. L. Marshall, *Catal. Lett.* **2011**, *141*, 498–506.
- [32] X. Huang, X. Qi, F. Boey, H. Zhang, *Chem. Soc. Rev.* **2012**, *41*, 666–686.
- [33] Y. B. Huang, Y. Fu, *Green Chem.* **2013**, *15*, 1095–1111.
- [34] Y. J. Gao, D. Ma, C. L. Wang, J. Guan, X. H. Bao, *Chem. Commun.* **2011**, *47*, 2432–2434.
- [35] M. Baghbanzadeh, L. Carbone, P. D. Cozzoli, C. O. Kappe, *Angew. Chem. Int. Ed.* **2011**, *50*, 11312–11359; *Angew. Chem.* **2011**, *123*, 11510–11561.
- [36] C. O. Kappe, *Chem. Soc. Rev.* **2008**, *37*, 1127–1139.
- [37] R. S. Oosthuizen, V. O. Nyamori, *Platinum Met. Rev.* **2011**, *55*, 154–169.
- [38] S. Barrientos-Ramírez, G. Montes de Oca-Ramírez, A. Sepúlveda-Escribano, M. M. Pastor-Blas, A. González-Montiel, F. Rodríguez-Reinoso, *Catal. Today* **2010**, *150*, 42–48.
- [39] D. Sun, X. Yan, J. Lang, Q. Xue, *J. Power Sources* **2013**, *222*, 52–58.

Received: October 21, 2013

Published online on March 19, 2014